



The Impact of Mechanical Activation on Nb Doped $\text{LiNi}_{0.8}\text{Co}_{0.1}\text{Mn}_{0.1}\text{O}_2$ Cathode Materials

Mona Maali, Alireza Babaei*, Abolghasem Ataie

School of Metallurgy and Materials Engineering, College of Engineering, University of Tehran, P.O. Box 11155-4563, Tehran, Iran.

Received: 16 February 2025; Accepted: 10 April 2025

*Corresponding author, E-mail: alireza.babaei@ut.ac.ir

ABSTRACT

The growing demand for lithium-ion batteries has prompted significant research into enhancing the performance and stability of cathode materials. This study investigates the effects of high-energy ball milling on the properties of niobium doped $\text{LiNi}_{0.8}\text{Co}_{0.1}\text{Mn}_{0.1}\text{O}_2$ (NMC811) cathode materials. X-ray diffraction (XRD), field emission scanning electron microscopy (FESEM), high-resolution transmission electron microscopy (HRTEM), energy dispersive X-ray spectroscopy (EDX), and X-ray photoelectron spectroscopy (XPS) were utilized to characterize the synthesized materials. Electrochemical performance was assessed through galvanostatic charge-discharge tests. In an un-milled NMC811 sample with Nb doping, the average primary particle size was 207 nm. Nb doping combined with ball milling further reduced the primary particle size to 150 nm. However, the use of ball milling, in addition to the excessive cationic mixing caused by Nb doping, negatively affected the rate capability probably due to the increased Nb content in the Li layer. The initial discharge capacity of NMC811 for the un-milled and ball milled samples was 161.9 and 140.6 mAh g^{-1} at 0.1C, respectively. After 100 cycles at 0.5 C, the capacity retention for the un-milled and milled samples were 66.2 and 89.8%, respectively within the voltage range of 2.8-4.3 V. This improvement in capacity retention is attributed to the reduced particle size and enhanced structural stability, which together help maintain better performance over extended cycling.

Keywords: Lithium-ion batteries, NMC811, Ball milling, Nb doping, Capacity retention.

1. Introduction

Lithium-ion batteries have become indispensable in modern technology, driving the transition toward sustainable energy systems. With the growing global population and rising demand for renewable energy and electric vehicles, these batteries are at the forefront of powering a cleaner and more efficient future. Their widespread application underscores their pivotal role in addressing global energy challenges [1-3].

Increasing the capacity of cathode materials is a highly effective strategy to improve the energy density of lithium-ion batteries, which is crucial for

catering to the needs of high-energy applications. Recently, the layered structure cathode materials, $\text{LiNi}_{(1-x-y)}\text{Mn}_x\text{Co}_y\text{O}_2$ (NMC), owing to their outstanding properties, have garnered significant attention [4, 5]. Increasing the Ni content in NMC could improve the specific capacity. Increased nickel content, particularly when $x > 0.6$, can impair the electrochemical performance as a result of thermal and structural instabilities [6, 7]. For example, during the process of calcination, it is common for Ni^{2+} ions in the precursors to face difficulties in completely oxidizing into Ni^{3+} , even when exposed to an oxygen atmosphere. As a

result, the Ni^{2+} ions have the ability to migrate to the Li sites in the produced cathode materials, as their radii are similar to that of Li^+ ions (0.69 Å for Ni^{2+} and 0.76 Å for Li^+). This phenomenon is referred to as “cation mixing” [8, 9]. This migration diminishes the accessibility of Li^+ ions for electrochemical extraction/intercalation and hinders the diffusion pathway of Li^+ ions, resulting in a decrease in capacity and slow kinetics in the electrode process [10, 11]. However, there are still practical difficulties that remain with high-nickel NMC cathode materials. One of these challenges is when these materials are first exposed to air, they react with CO_2 and H_2O , forming impurities such as LiOH and Li_2CO_3 on their surface. These impurities limit the passage of Li ions and electrons, leading to a decrease in capacity.

It has been shown that doping with suitable ions effectively reduces the structural degradation of cathodes containing high nickel content. The larger ionic radius of Nb^{5+} (0.64 Å) compared to that of Ni^{3+} (0.56 Å) leads to an increase in lattice parameters. As a result, Nb doping creates numerous Li^+ channels in the layered structure [12, 13]. Nb^{5+} enhances the electrochemical characteristics and Li^+ mobility. Therefore, Nb^{5+} is a suitable option for different cathodes [14, 15].

In general, the electrochemical performance of NMCs depends on the specific conditions under which they are prepared and synthesized. Mechanical activation via high-energy ball milling is well-known for reducing particle size and improving material properties, particularly for energy-related materials [16-18]. Factors such as milling speed, milling time, and the ball-to-powder ratio (BPR) influence the energy transfer to the powder, which in turn affects various properties such as particle size, surface area, and electrochemical characteristics like charge/discharge capability and reversibility [19-21].

This study systematically investigates the effect of high-energy ball milling as an innovative approach for Nb doping in NMC811 cathode materials, with a detailed focus on the structural/morphological properties and their impact on electrochemical performance.

2. Experimental procedure

2.1. Materials synthesis

To obtain $\text{LiNi}_{0.8}\text{Co}_{0.1}\text{Mn}_{0.1}\text{O}_2$, the first step involves producing a $\text{Ni}_{0.8}\text{Co}_{0.1}\text{Mn}_{0.1}(\text{OH})_2$ precursor through the co-precipitation method [22]. To obtain the $\text{Ni}_{0.8}\text{Co}_{0.1}\text{Mn}_{0.1}(\text{OH})_2$, the synthesis was carried out in a stirred tank reactor under a nitrogen atmosphere. Reagent-grade $\text{NiSO}_4 \cdot 6\text{H}_2\text{O}$, $\text{CoSO}_4 \cdot 7\text{H}_2\text{O}$, and $\text{MnSO}_4 \cdot \text{H}_2\text{O}$ (Merck) were dissolved in a specific volume of deionized water with a molar ratio of 8:1:1, resulting in a solution with a concentration of 2 mol l^{-1} . Injection of this solution was meticulously conducted using peristaltic pumps, by slowly pumping into the reactor (600 mL volume) containing NH_4OH (Merck) with a concentration of 1 mol l^{-1} . Additionally, NH_4OH solution with concentrations of 0.75 mol l^{-1} was separately pumped into the reactor to act as a chelating agent. The pH was rigorously maintained at 11.3. The molar ratio of NaOH (Samchun) to the total molar amount of sulfates was fixed at 2 mol l^{-1} , with automatic injection into the reactor based on the pH value within. The precipitation reaction was conducted at a constant temperature of 58°C and a fixed stirring speed of 1000 rpm. After 44 hours of the co-precipitation process, the precipitates were filtered, followed by multiple washes with deionized water. Once the $\text{Ni}_{0.8}\text{Co}_{0.1}\text{Mn}_{0.1}(\text{OH})_2$ hydroxide was obtained, it was used for the subsequent steps. $\text{Ni}_{0.8}\text{Co}_{0.1}\text{Mn}_{0.1}(\text{OH})_2$ was mixed with 1 wt% Nb_2O_5 in an absolute ethanol solution, and then dried. $\text{LiOH} \cdot \text{H}_2\text{O}$ was subsequently added in a 1:1.07 ratio to compensate for lithium loss during high-temperature calcination. Additionally, mechanical activation was performed using a planetary ball mill to mix the $\text{Ni}_{0.8}\text{Co}_{0.1}\text{Mn}_{0.1}(\text{OH})_2$ precursor with $\text{LiOH} \cdot \text{H}_2\text{O}$, 1 wt% Nb_2O_5 , and a specific amount of toluene. Both the vial and balls were composed of hardened chromium steel. The ball to powder weight ratio was 20. The milling was paused every hour to allow the vials to cool down. Subsequently, the un-milled and milled samples underwent heating at 480°C for 5 hours, followed by 12 hours at 800°C under an oxygen atmosphere. Table 1 presents an overview of the process conditions.

Table 1- Processing conditions of the samples

Ball milling conditions					
Sample identity	Milling speed	Milling time	BPR	Ball diameter	Calcination Temperature (°C)
	(rpm)	(hours)		(mm)	
NMC	-	-	-	-	480/800
Milled-NMC	250	5	20:1	10	480/800

2.2. Materials characterization

The X-ray diffraction (XRD) measurement is carried out to analyze the crystalline structure (Rigaku SmartLab, 9kW, Cu K α , λ = 0.154 nm). The morphology of the samples was examined by field emission scanning electron microscope (FESEM, TESCAN Mira3 instrument). The primary particle size was determined from the FESEM images using ImageJ software. X-ray photoelectron spectroscopy (XPS) was carried out using a PREVAC Sp. z o. o. UHV system equipped with an Al anode (300W). Survey scans were performed at a pass energy of 200 eV with 3 iterations, while high-resolution scans were acquired at a pass energy of 50 eV with 20 iterations. The structure and morphology of the material were examined in a FEI Tecnai F30 G² STwin (300 kV, FEG) using electron diffraction and high-resolution transmission electron microscopy (HRTEM), and high-angle annular dark-field scanning TEM (HAADF-STEM) imaging. Energy-dispersive X-ray spectroscopy (EDX) mapping was conducted with a Si/Li detector (EDAX) in STEM mode.

2.3. Electrochemical characterizations

The electrochemical performance assessment of the cathode materials was examined using CR-2032 coin-type half-cells. The positive electrodes were prepared by mixing the active material powder, Super P carbon black as the conductive agent, and polyvinylidene fluoride (PVDF) binder in a weight ratio of 8:1:1. N-methyl pyrrolidinone (NMP) solvent was added to the mixture to create a uniform slurry. This slurry was then coated onto aluminum foil and dried in a vacuum oven at 100°C for 24 hours. The mass loading of all cathode samples was maintained at 4.3 ± 3 g cm⁻². Lithium foil and Celgard microporous polypropylene film were employed as the anode and separator, respectively. The electrolyte was obtained by dissolving 1 M LiPF₆ in a solution of ethylene carbonate (EC) and dimethyl carbonate (DMC) in equal volume ratios. Prior to electrochemical testing, all prepared half-cells were allowed to equilibrate at room temperature for 24 hours. Galvanostatic charge-discharge tests at various C-rates (1C = 180 mA g⁻¹) within the voltage range of 2.8–4.3 V (versus Li/Li⁺), were carried out on a battery test system (Neware) at room temperature. The cells underwent 4 formation cycles at 0.05C followed by 3 cycles at 0.1C for stabilization. Afterward, the batteries were cycled at 0.5C for 100 cycles.

3. Results and discussion

Fig. 1(a) illustrates the XRD patterns of the NMC and Milled-NMC samples. The diffraction peaks of both samples are indexed to the structure

of LiNiO₂ phase (JCPDS card No. 89-3601) with a space group of Rm, confirming the layered structure of the synthesized powder [23]. As shown in Fig. 1(b) and (c), the split of (006)/(012) and (018)/(110) reflections are observed, showing a well-established layered structure [24]. In the magnified (003) reflections shown in Fig. 1(d), the (003) peak for the Milled-NMC sample shifts toward lower angles compared to the NMC sample. This shift suggests an increase in unit cell volume, attributed to the successful doping of Nb, which expands the interplanar spacing. Such expansion likely enhances the Li-ion diffusion coefficient [12, 25]. It should be noted that since the milled samples underwent post-milling heat treatment, residual strain from ball milling was likely relieved, leaving Nb⁵⁺ doping as the primary factor responsible for the observed peak shifts. Fig. 1(e-f) presents the Rietveld refinement patterns from XRD data for the NMC and Milled-NMC samples, with corresponding crystallographic data summarized in Table 2. The R_{wp} values are below 5%, indicating the validity of the refinement results. Generally, the $I_{(003)}/I_{(104)}$ intensity ratio reflects the degree of Li⁺/Ni²⁺ cation mixing, with values below 1.2 indicating significant cation mixing [26]. For the NMC and Milled-NMC samples, the $I_{(003)}/I_{(104)}$ ratios are 1.57 and 1.35, respectively suggesting minimal cation mixing and a well-maintained layered structure. The substitution of Nb⁵⁺ ions induces local lattice distortion, increasing the unit cell volume in the Milled-NMC sample. Additionally, Nb doping increases the c lattice parameter in this sample. This enhancement is attributed to the replacement of smaller Ni³⁺ (0.056 nm), Co³⁺ (0.055 nm), and Mn⁴⁺ (0.053 nm) ions with larger Nb⁵⁺ ions (0.064 nm), as well as the stronger Nb–O bond compared to the metal–O bonds [27, 28].

The chemical valence states on the surfaces of the NMC and Milled-NMC samples were analyzed using XPS, and the corresponding results are presented in Fig. 2. The O 1s spectra exhibit two distinct peaks: 528 eV, corresponding to lattice oxygen (O_{lattice}), and 532.5 eV, attributed to adsorbed oxygen (O_{adsorbed}). The O_{adsorbed} peak originates from active oxygen species present on the surface, including LiOH, Li₂CO₃, and LiHCO₃, while O_{lattice} is associated with metal-oxygen bonding. This peak assignment is consistent with previous studies [29]. The results indicate that the Milled-NMC sample exhibits a lower O_{lattice} content compared to NMC. This reduction in O_{lattice} suggests a higher degree of surface contamination with LiOH and Li₂CO₃, likely due to increased exposure to moisture and CO₂ during the ball milling process. Ni-rich NMC materials undergo reactions with CO₂ and H₂O, leading to the formation of LiOH and Li₂CO₃ as the primary surface impurities. In general,

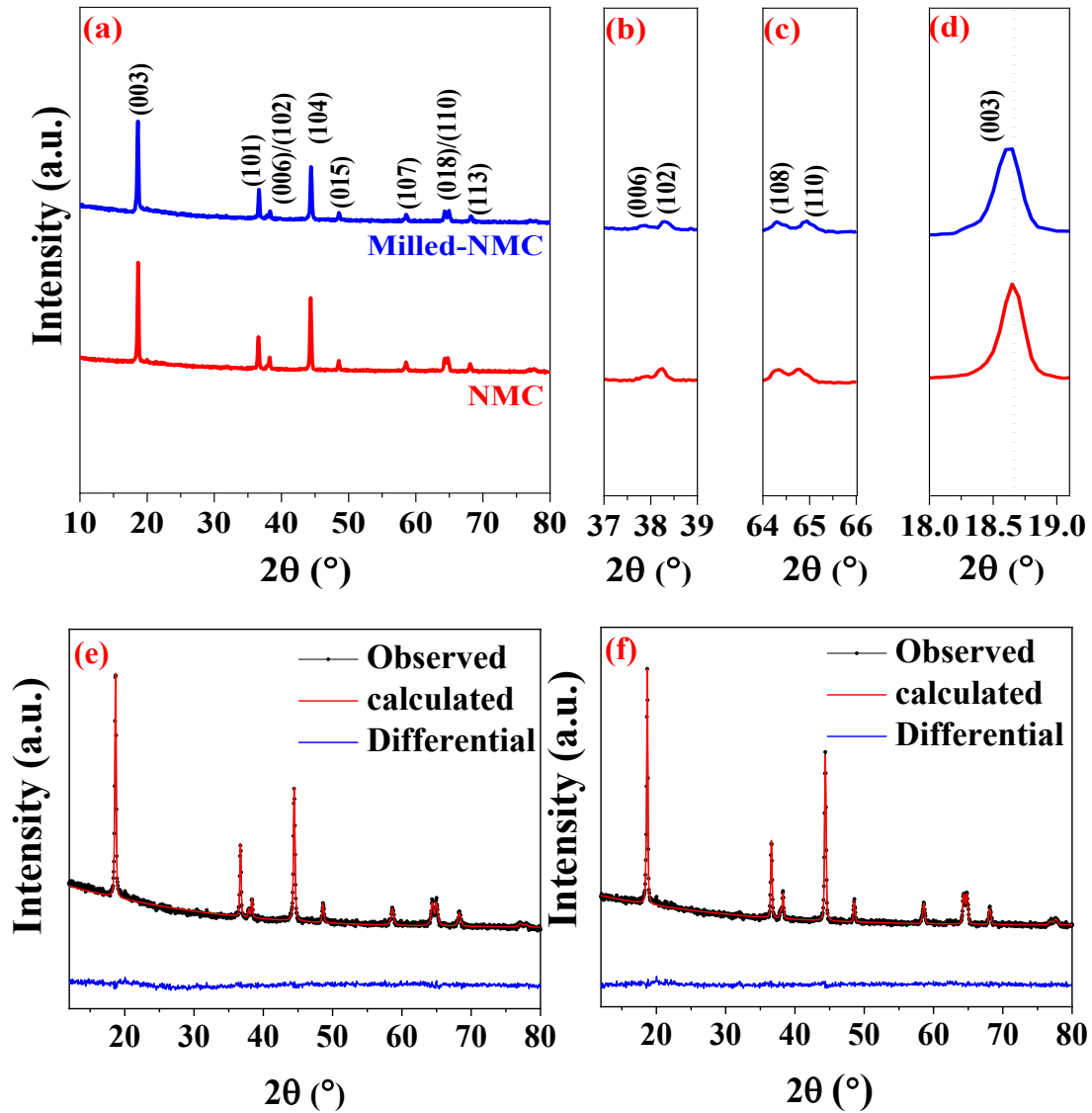


Fig. 1- (a) XRD patterns of the $\text{LiNi}_{0.8}\text{Co}_{0.1}\text{Mn}_{0.1}\text{O}_2$ samples from bottom to top in order: NMC and Milled-NMC, (b) Magnified XRD patterns of (006)/(102), (c) (108)/(110) and (d) (003) reflections. XRD Rietveld refinement of (e) NMC and (f) Milled-NMC.

Table 2- XRD Parameters and Rietveld Refinement results of samples NMC and Milled-NMC

Sample identity	R_{wp} (%)	c (Å)	a (Å)	V (Å ³)	$I_{(003)} / I_{(104)}$
NMC	2.89	14.2356	2.8689	101.46	1.57
Milled-NMC	2.01	14.2383	2.8731	101.78	1.35

ball milling enhances mixing and promotes a more homogeneous distribution of components. However, the observed decrease in O_{lattice} implies that ball milling may also facilitate the formation of lithium-containing surface impurities.

Fig. 3 shows FESEM images of the NMC and Milled-NMC samples. As shown in Fig. 3(a-b), the secondary particles resulting from Nb doping are clustered and less distinct from one another. The contraction of the primary particles in the sample shown in Fig. 3(c) is intensified due to the ball milling process. The contraction of primary particles may be due to the significantly higher dissociation energy of the Nb-O bond ($\Delta H_{f,298}(\text{Nb-O}) = 753 \text{ kJ mol}^{-1}$) compared to the Ni-O bond ($\Delta H_{f,298}(\text{Ni-O}) = 391 \text{ kJ mol}^{-1}$), Co-O bond ($\Delta H_{f,298}(\text{Co-O}) = 368 \text{ kJ mol}^{-1}$), and Mn-O bond ($\Delta H_{f,298}(\text{Mn-O}) = 402 \text{ kJ mol}^{-1}$) [29, 30]. High-valence elements like Nb^{5+} , Ta^{5+} , Mo^{6+} , and W^{6+} typically exhibit limited solubility within the crystal structure of Ni-rich NMC. They tend to segregate at the grain boundaries, which helps to suppress the coarsening of primary particles [15]. As shown in Fig. 1S(a-b), the primary NMC particles formed with an approximate size of 207 nm, when ball milling is used for Nb doping, the primary particle size is reduced to 150 nm. These changes in particle size can be attributed to the combined effects of ball milling and Nb doping exhibits the smallest primary particle size and the narrowest distribution. This size reduction can increase the surface area of the material, which is beneficial for enhancing reaction kinetics in the cathode. A smaller particle size generally shortens the Li^+ diffusion path, facilitating the rapid insertion and extraction of Li^+ ions. Additionally, a compact

structure enhances structural stability, helping to maintain structural integrity during the cycling process.

Fig. 4(a-d) shows the TEM images of the NMC and Milled-NMC samples. The TEM images do not reveal any other impurity phases, which indicates that all samples possess well-layered structures. Fig. 2S(a-b) displays high-resolution transmission electron microscopy (HRTEM) images, revealing that the material adopts a rhombohedral structure characterized by the R-3m space group, consistent with the XRD results. The d_{003} spacing of the Milled-NMC sample is 0.481 nm, slightly larger than that of the NMC sample, which measures 0.476 nm. Doping Nb via high-energy ball milling results in a slight expansion of the lattice along the c-axis direction. This observation is consistent with the XRD results. An increase in d-spacing, as observed in the Milled-NMC sample, can sometimes facilitate lithium-ion diffusion by providing larger channels. However, if the Nb ions are not uniformly distributed or create irregularities within the lattice, these larger channels can become less effective or even obstruct lithium-ion pathways. This irregularity can hinder the smooth movement of lithium ions, reducing their capacity. In Fig. 4(c), to check the distribution of the elements in the samples, EDX mapping was performed in Scanning TEM (STEM) mode on the NMC sample. As it shows, Ni, Co and Mn are uniformly distributed. The elemental composition assessed by EDX for both samples indicates a cation ratio of Ni:Mn:Co as 8:1:1. The average amount of Nb in NMC and Milled-NMC samples is 0.6 and 1.16%, respectively.

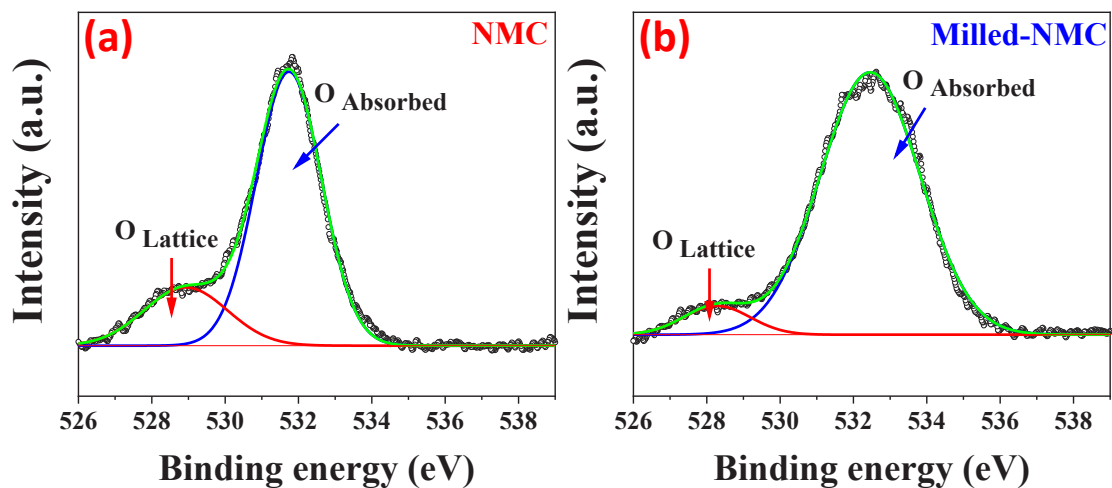


Fig. 2- XPS spectra of O 1s for the samples: (a) NMC and (b) Milled-NMC.

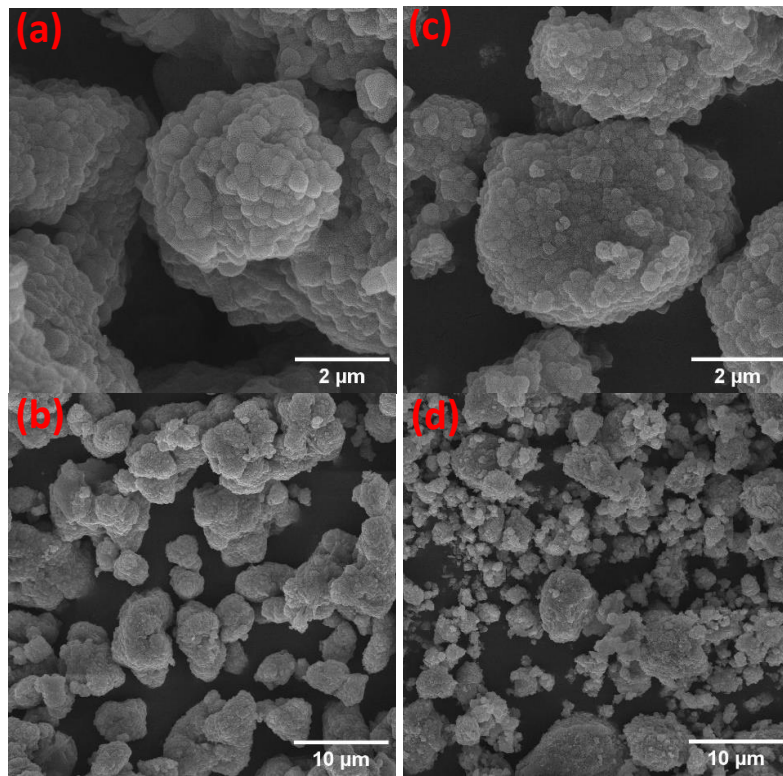


Fig. 3- FESEM images of the NMC811 samples: (a, b) NMC and (c, d) Milled-NMC.

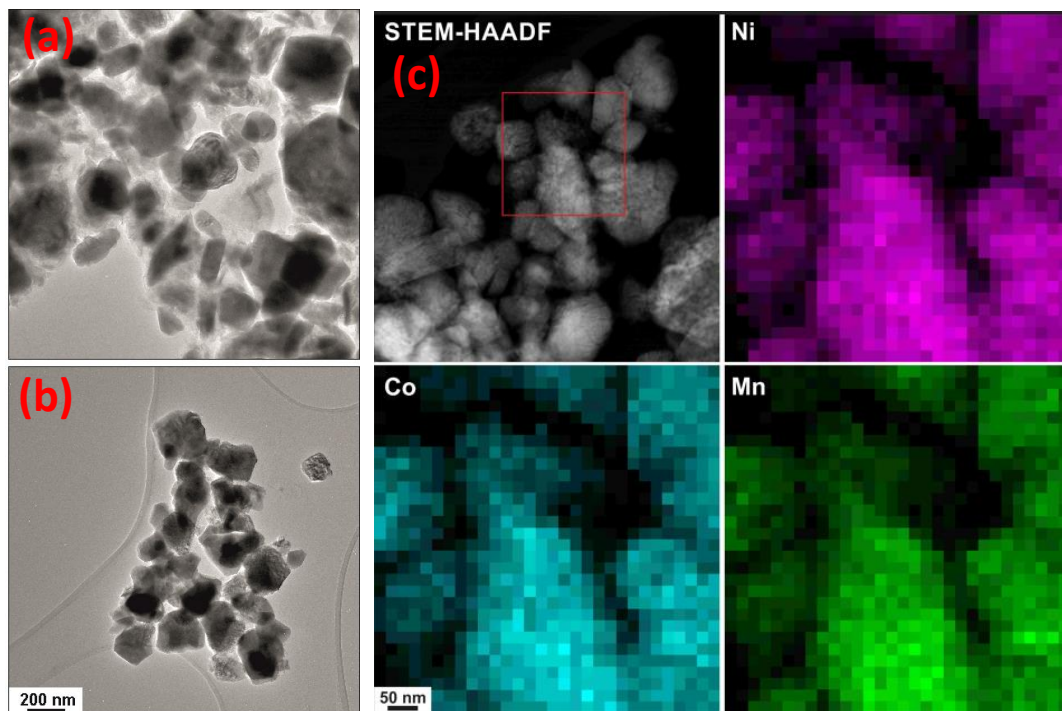


Fig. 4- The TEM images of the NMC811 samples: (a) NMC, (b) Milled-NMC, and (e) STEM-EDX mapping of the NMC sample.

In Fig. 5(a), the rate performance of cell batteries made with NMC and Milled-NMC cathodes at different cycling rates (0.1C to 2.0C) between 2.8 and 4.3 V at room temperature is compared, showing specific discharge capacities of 161.9 and 140.62 mAh g⁻¹ at 0.1C, respectively. The NMC sample exhibits a higher discharge capacity compared to the Milled-NMC sample. The capacity recovery rate of NMC and Milled-NMC is 99.5 and 98.3%, respectively. It was reported that the rate capability of cathode materials is determined by particle size and the lithium-ion diffusion coefficient (D_{Li^+}) [31]. The decrease in the performance rate of the Milled-NMC sample can be attributed to the fact that a higher c value provides broader Li⁺ transfer pathways in the network, and smaller primary particles shorten the transfer paths to promote the diffusion of Li⁺ ions, while the excessive degree of cation mixing in the Milled-NMC sample leads to more Ni²⁺ ions occupying Li⁺ sites, causing a decline in capacity and rate performance. It is worth noting that the extremely low discharge capacity at various rates indicates poor rate performance caused by the presence of LiOH/ Li₂CO₃ impurities as shown in XPS results. Fig. 5(b) presents the initial charge-discharge profiles of NMC and Milled-NMC at a rate of 0.1C. The curves of both samples exhibit stability and typical electrochemical behavior, suggesting that no new phases were formed during the initial charging and discharging processes. The Coulombic efficiencies (CEs) of NMC and Milled-NMC are 98.6% and 98.8%, respectively, showing only a minimal difference between them.

Fig. 6(a) illustrates the cycling performances of the NMC and Milled-NMC cathodes at 0.5 C over 100 cycles at room temperature within the voltage range of 2.8 to 4.3 V (vs. Li/Li⁺) following an initial activation process consisting of 4 cycles at 0.05C and 3 cycles at 0.1C. Herein, the NMC and Milled-

NMC cathodes exhibited initial discharge capacities of 100.8 and 93.0 mAh g⁻¹, respectively. When ball milling is used for Nb doping, the sample exhibited a lower initial discharge capacity. Additionally, after 100 charge/discharge cycles, the capacity retention rates for the NMC and Milled-NMC cathodes were 66.2 and 89.8%, respectively. These results confirm that, in addition to the severe Li/Ni mixing mentioned earlier, the improved capacity retention but significantly poorer rate performance of the Milled-NMC compared to the NMC sample may be attributed to the high niobium (Nb) content in the lithium (Li) layer resulting from the ball milling process. As shown in previous studies, the excessive integration of dopants has been linked to a decline in electrochemical performance [32]. Differential capacity (dQ/dV) plots versus electrode potential for NMC and Milled-NMC samples after cycles (1 and 100) at 0.5 C rates are shown in Fig. 6(b-c) to illustrate the differences in cycle stability among the two cathodes. For both samples, as the charge-discharge cycles continue, the peaks on the positive side shift towards higher potentials, while the peaks on the negative side shift in the opposite direction. This behavior indicates that the excessive increase in the potential required for the extraction and insertion of Li⁺ ions during charging and discharging causes phase transitions to be continuously delayed. Relating to the improved cycling performance mentioned above, the Milled-NMC sample shows a reduced ΔV between the 1st and 100th cycles, indicating more stable oxidation of the transition metals and more reversible lithium extraction from the layered oxides. Another important measure is the disparity in potential (ΔV) between the oxidation and reduction peaks during the first cycle. This disparity is smaller for the Milled-NMC, suggesting a decrease in polarization in these cathodes.

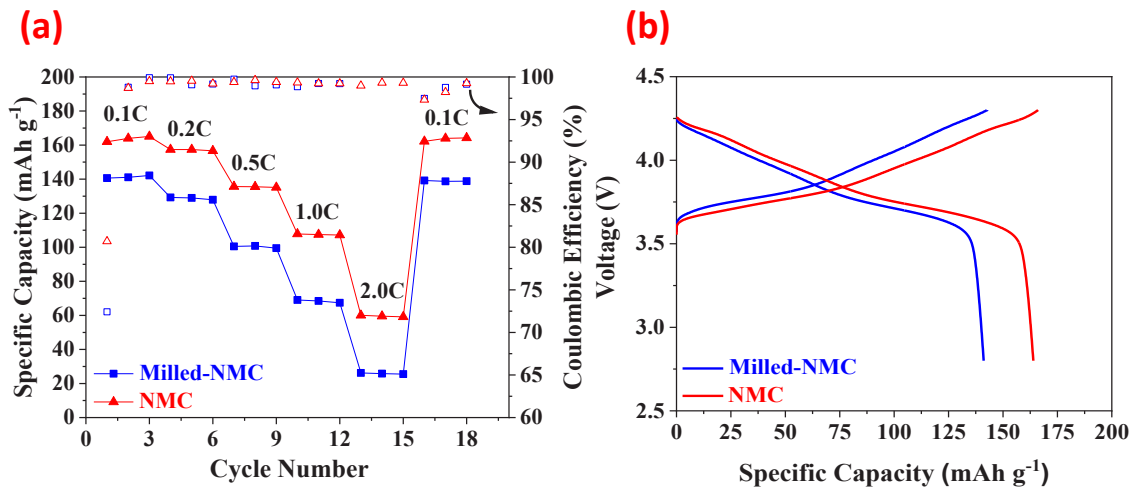


Fig. 5- (a) Rate performance, (b) The second charge/discharge curves of samples NMC and Milled-NMC at 0.1C.

4. Conclusions

This study examines the effects of high-energy ball milling on the properties of Nb doping in $\text{LiNi}_{0.8}\text{Co}_{0.1}\text{Mn}_{0.1}\text{O}_2$ cathode materials. Nb doping via ball milling reduces the NMC particle size from 207 to 150 nm, intensifying the primary particles' cohesion. XRD results indicate that the unit cell volume is increased via ball milling due to successful Nb doping, which also leads to a slight increase in the d_{003} spacing, indicating a minor expansion of the lattice along the c-axis. The high-energy ball milling process played a crucial role in controlling particle size, structure,

and electrochemical performance, reducing ΔV between the 1st and 100th cycles, which indicates stable oxidation and reversible lithium extraction. This improved capacity retention from 66.2 to 89.8% through shorter Li^+ transport paths. However, the high level of cation mixing in the Milled-NMC sample leads to increased occupancy of Li^+ sites by Ni^{2+} ions, leading to a decrease in both capacity and rate performance. Despite these limitations, this study highlights the potential of combining Nb doping and ball milling as a promising strategy for optimizing high-Ni NMC cathodes.

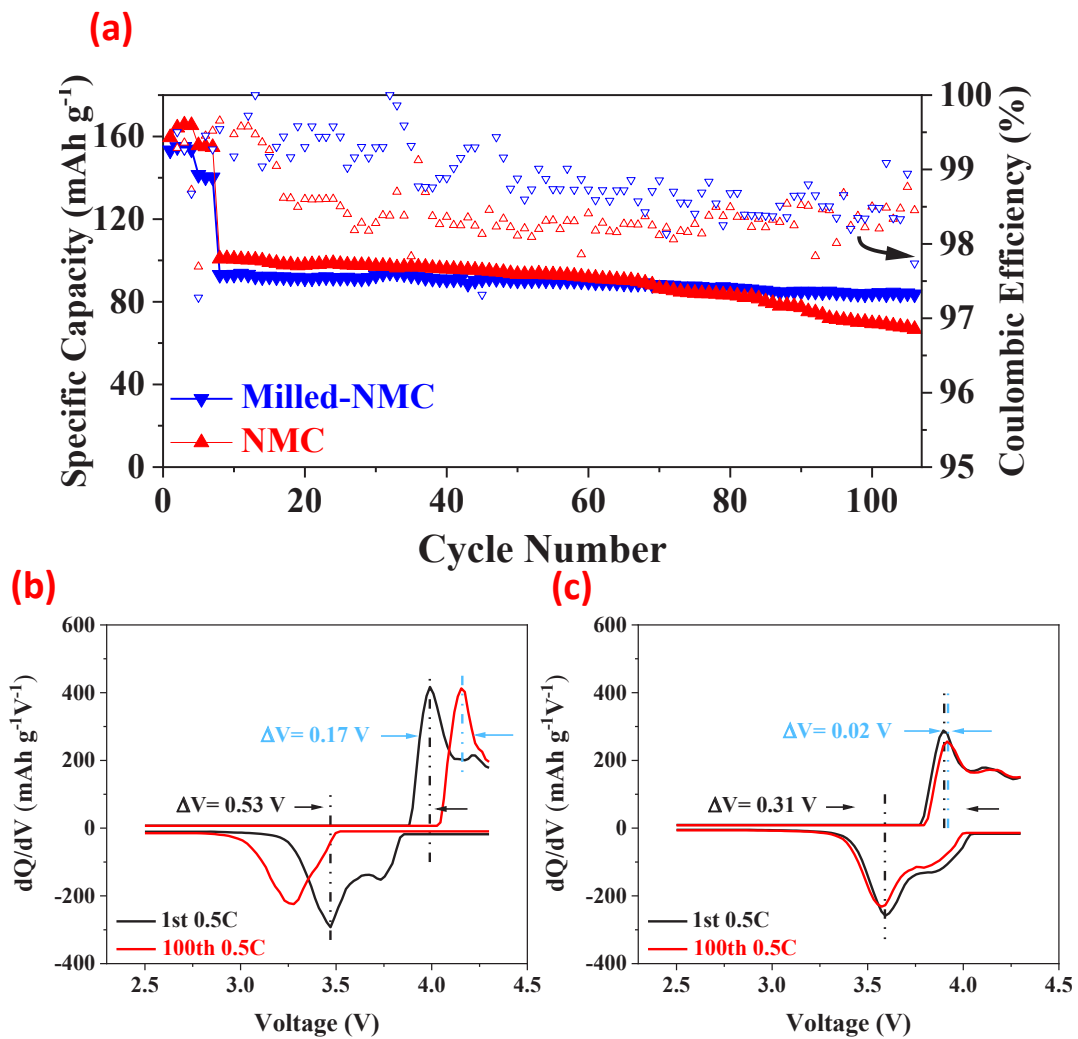


Fig. 6- (a) Cycling performance curves of NMC and Milled-NMC cathodes at 0.5C, after 4 cycles at 0.05C and 3 cycles at 0.1C. Differential capacity vs voltage curves of (b) NMC and (c) Milled-NMC.

References

- Alolaywi H, Uzun K, Cheng Y-T. Low porosity NMC622 and NMC811 electrodes made by severe calendaring. *Journal of Energy Storage*. 2025;105:114559.
- Lecompte M, Bernard J, Calas E, Richardet L, Guignard A, Duclaud F, et al. Experimental assessment of high-energy high nickel-content NMC lithium-ion battery cycle life at cold temperatures. *Journal of Energy Storage*. 2024;94:112443.
- Saaïd FI, Kasim MF, Winie T, Elong KA, Azahidi A, Basri ND, et al. Ni-rich lithium nickel manganese cobalt oxide cathode materials: A review on the synthesis methods and their electrochemical performances. *Heliyon*. 2024;10(1).
- Lu H, Zhou H, Svensson AM, Fossdal A, Sheridan E, Lu S, Vullum-Bruer F. High capacity Li [Ni_{0.8}Co_{0.1}Mn_{0.1}]O₂ synthesized by sol-gel and co-precipitation methods as cathode materials for lithium-ion batteries. *Solid State Ionics*. 2013;249:105-11.
- Guo J, Li Y, Meng J, Pedersen K, Gurevich L, Stroe D-I. Understanding the mechanism of capacity increase during early cycling of commercial NMC/graphite lithium-ion batteries. *Journal of Energy Chemistry*. 2022;74:34-44.
- Wu F, Tian J, Su Y, Wang J, Zhang C, Bao L, et al. Effect of Ni²⁺ content on lithium/nickel disorder for Ni-rich cathode materials. *ACS applied materials & interfaces*. 2015;7(14):7702-8.
- Guo Y, Miao M, Wang Y-X, Yan C, Liu J, Cao Y, et al. A high-voltage and low-solvating electrolyte towards promising micro-Si/Ni-rich NMC full cells. *Energy Storage Materials*. 2024;67:103258.
- Wei H-x, Tang L-b, Wang Z-y, Luo Y-h, He Z-j, Yan C, et al. Comprehensive understanding of Li/Ni intermixing in layered transition metal oxides. *Materials Today*. 2021;51:365-92.
- Williams E, Kendrick E, editors. *Improved Cycle Life and Determination of Li Ion Transport Parameters in Mixed Cation Doped Ni-Rich NMC*. Electrochemical Society Meeting Abstracts 244; 2023: The Electrochemical Society, Inc.
- Wang X, Ding YL, Deng YP, Chen Z. Ni-rich/Co-poor layered cathode for automotive Li-ion batteries: promises and challenges. *Advanced Energy Materials*. 2020;10(12):1903864.
- Luchkin SY, Kirsanova MA, Aksyonov DA, Lipovskikh SA, Nikitina VA, Abakumov AM, Stevenson KJ. Cycling-driven electrochemical activation of Li-rich NMC positive electrodes for Li-ion batteries. *ACS Applied Energy Materials*. 2022;5(6):7758-69.
- Kim Y-R, Yoo Y-W, Hwang D-Y, Shim T-Y, Kang C-Y, Park H-J, et al. Effect of niobium doping to enhance electrochemical performances of LiNi_{0.8}Co_{0.1}Mn_{0.1}O₂ cathode material. *Solid State Ionics*. 2023;389:116108.
- Xin F, Goel A, Chen X, Zhou H, Bai J, Liu S, et al. Electrochemical characterization and microstructure evolution of Ni-rich layered cathode materials by niobium coating/substitution. *Chemistry of Materials*. 2022;34(17):7858-66.
- Zhang L, Xiao L, Zheng J, Wang H, Chen H, Zhu Y. Effect of Nb⁵⁺ doping and LiNbO₃ coating on the structure and surface of a LiNi_{0.8}Mn_{0.2}O₂ cathode material for lithium-ion batteries. *Journal of The Electrochemical Society*. 2021;168(11):110528.
- Nunes BN, van den Bergh W, Strauss F, Kondrakov A, Janek J, Brezesinski T. The role of niobium in layered oxide cathodes for conventional lithium-ion and solid-state batteries. *Inorganic Chemistry Frontiers*. 2023;10(24):7126-45.
- Tian Y. *Synthesis and Characterization of Mg, Nb, Ti-Doped LiNiO₂ Cathode Material for Li-Ion Batteries*: Illinois Institute of Technology; 2022.
- Pan T, Alvarado J, Zhu J, Yue Y, Xin HL, Nordlund D, et al. Structural degradation of layered cathode materials in lithium-ion batteries induced by ball milling. *Journal of the electrochemical society*. 2019;166(10):A1964.
- Hodaei A, Ataie A, Mostafaei E. Intermediate milling energy optimization to enhance the characteristics of barium hexaferrite magnetic nanoparticles. *Journal of Alloys and Compounds*. 2015;640:162-8.
- Kim S-B, Kim S-J, Kim C-H, Kim W-S, Park K-W. Nanostructure cathode materials prepared by high-energy ball milling method. *Materials letters*. 2011;65(21-22):3313-6.
- Murty B, Rao MM, Ranganathan S. Milling maps and amorphization during mechanical alloying. *Acta Metallurgica et Materialia*. 1995;43(6):2443-50.
- Mahdikhah V, Ataie A, Akbari Moayer H, Molaei MJ, Babaei A. Magnetic and photocatalytic properties of CoFe₂O₄/Ni nanocomposites. *Journal of Electroceramics*. 2022:1-16.
- Wu Z, Zhou Y, Zeng J, Hai C, Sun Y, Ren X, et al. Investigating the effect of pH on the growth of coprecipitated Ni_{0.8}Co_{0.1}Mn_{0.1}(OH)₂ agglomerates as precursors of cathode materials for Li-ion batteries. *Ceramics International*. 2023;49(10):15851-64.
- Ilyas S, Srivastava RR, Kim H. Cradle-to-cradle recycling of spent NMC batteries with emphasis on novel Co²⁺/Ni²⁺ separation from HCl leached solution and synthesis of new ternary precursor. *Process Safety and Environmental Protection*. 2023;170:584-95.
- Bandpey M, Dorri M, Babaei A, Zamani C, Bortolotti M. Improved Electrochemical Performance of the Cation-Disordered NMC Cathode of Lithium-Ion Batteries by Lithium Phosphate Coating. *ACS Applied Energy Materials*. 2023;6(15):7974-84.
- Li X, Lai T, Sheng A, Yang J, Li Y, Xiao S, et al. Effects of Nb-doping on cycle life, self-discharge and crack resistance of Ni-rich LiNi_{0.94}Co_{0.02}Al_{0.04}O₂ cathode for Li-ion batteries. *Journal of Energy Storage*. 2023;72:108262.
- Zhang X, Jiang W, Mauger A, Gendron F, Julien C. Minimization of the cation mixing in Li_{1+x}(NMC) 1-xO₂ as cathode material. *Journal of Power Sources*. 2010;195(5):1292-301.
- Wang J, Liu C, Wang Q, Xu G, Miao C, Xu M, et al. Investigation of W⁶⁺-doped in high-nickel LiNi_{0.83}Co_{0.11}Mn_{0.06}O₂ cathode materials for high-performance lithium-ion batteries. *Journal of Colloid and Interface Science*. 2022;628:338-49.
- Liu S, Chen X, Zhao J, Su J, Zhang C, Huang T, et al. Uncovering the role of Nb modification in improving the structure stability and electrochemical performance of LiNi_{0.6}Co_{0.2}Mn_{0.2}O₂ cathode charged at higher voltage of 4.5 V. *Journal of power sources*. 2018;374:149-57.
- Wang J, Yi Z, Liu C, He M, Miao C, Li J, et al. Revealing the effect of Nb⁵⁺ on the electrochemical performance of nickel-rich layered LiNi_{0.83}Co_{0.11}Mn_{0.06}O₂ oxide cathode for lithium-ion batteries. *Journal of Colloid and Interface Science*. 2023;635:295-304.
- Yang Z, Xiang W, Wu Z, He F, Zhang J, Xiao Y, et al. Effect of niobium doping on the structure and electrochemical performance of LiNi_{0.5}Co_{0.2}Mn_{0.3}O₂ cathode materials for lithium ion batteries. *Ceramics International*. 2017;43(4):3866-72.
- Liu J, Chen H, Xie J, Sun Z, Wu N, Wu B. Electrochemical performance studies of Li-rich cathode materials with different primary particle sizes. *Journal of Power Sources*. 2014;251:208-14.
- Chu M, Huang Z, Zhang T, Wang R, Shao T, Wang C, et al. Enhancing the electrochemical performance and structural stability of Ni-rich layered cathode materials via dual-site doping. *ACS Applied Materials & Interfaces*. 2021;13(17):19950-8.